



Electrochemical investigation of $\text{La}_{0.4}\text{Sr}_{0.6}\text{TiO}_3$ synthesized in air for SOFC application

Jiaqi Cheng¹ · Junyi Gong¹ · Shuai Yue¹ · Yao Jiang¹ · Xiangjun Hou¹ · Jianjun Ma¹ · Yali Yao² · Cairong Jiang¹

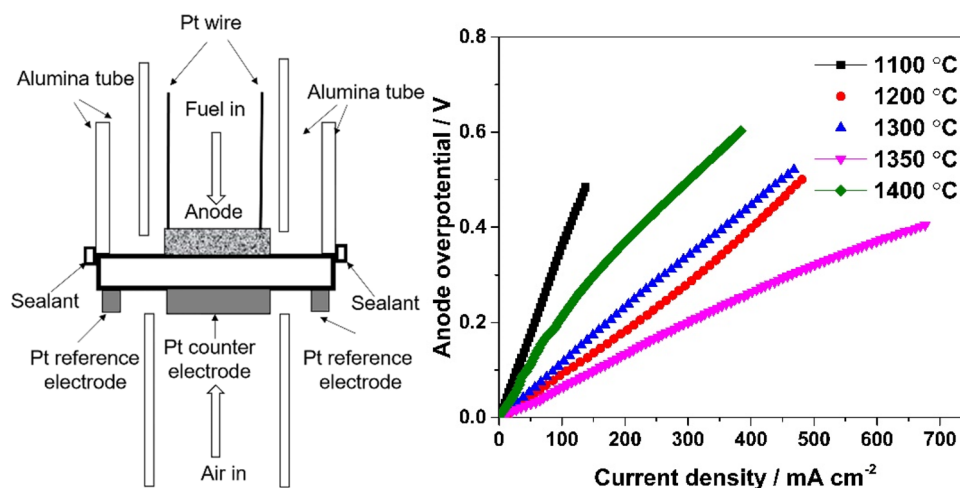
Received: 26 November 2020 / Accepted: 20 April 2021 / Published online: 11 May 2021
© The Author(s), under exclusive licence to Springer Nature B.V. 2021

Abstract

La-doped titanate materials have been widely investigated as alternative Ni-free anodes for solid oxide fuel cells (SOFCs). In this study, $\text{La}_{0.4}\text{Sr}_{0.6}\text{TiO}_3$ (LST) was synthesized using the solid-state reaction method and calcined in air. A three-electrode mode was applied to measure the electrochemical performance of LST-yttria-stabilized zirconia (YSZ) composite anode by testing its impedance spectra and the anode overpotential. The electrochemical behavior is strongly dependent on the sintering temperature and the YSZ content. The lowest polarization resistance of $0.26 \Omega \text{ cm}^2$ in 97% $\text{H}_2/3\% \text{H}_2\text{O}$ was obtained on the anode sintered at 1350°C when adding 60 wt% YSZ. The cell with the LST–YSZ anode was operated at 10,000 ppm $\text{H}_2\text{S-H}_2$ at 850°C for more than 10 h, and it exhibited excellent sulfur-tolerant ability. The LST–YSZ anode sintered in air instead of reducing condition is probably a potential anode material for SOFCs.

Graphic abstract

The electrochemical performance of LST–YSZ anode depends strongly on the YSZ content and the calcination temperature tested by overpotential in a three-electrode mode.



Keywords Composite anode · Sintering temperature · Three-electrode mode · Overpotential · Sulfur tolerant

✉ Jianjun Ma
jjma@suse.edu.cn

✉ Cairong Jiang
crjiang@suse.edu.cn

Extended author information available on the last page of the article

1 Introduction

Solid oxide fuel cells (SOFCs) offer an environmentally friendly technology that can be used to convert the chemical energy of fuels into electricity with high efficiency [1], as it is not subject to Carnot cycle limitation [2, 3]. The most

widely used anode materials for SOFCs are the Ni-based anodes, which offer high electronic conductivity and sufficient catalytic activity towards the oxidation of hydrogen on the anode side [4, 5]. Based on the Ni/yttria-stabilized zirconia (YSZ) cermet anode, the SOFC with these anodes generated a maximum power density of up to 1.8 W cm^{-2} at $800 \text{ }^\circ\text{C}$ measured in the experiments when using hydrogen as the fuel [6]. Unfortunately, poor redox stability, low tolerance to sulfur, and carbon coking of Ni are the main issues in terms of commercial applications, if hydrocarbon is used as the fuel [7–9]. In terms of sulfur poisoning, the polarization resistance of the nickel anode rises by about 42% from 3.5 to $6 \text{ } \Omega \text{ cm}^2$ at $900 \text{ }^\circ\text{C}$, even though sulfur is only 1 ppm [10].

The development of the ceramic anode as a substitute for the Ni-based cermet would provide significant profit for SOFCs. To date, some perovskite oxides, such as Cr-based [11], Ti-based materials, and other perovskites ($\text{Sr}_2\text{Mg}_{1-x}\text{Mn}_x\text{MoO}_{6-8}$) have been developed for use with SOFCs [12, 13]. Recently, La or Y-doped strontium titanate (SrTiO_3) received intensive research interest due to its electronic conductivity, Thermal Expansion Coefficient (TEC) compatibility with YSZ [14], and high resistance to sulfur [15]. Of these two types of materials, La-doped SrTiO_3 has a higher doping content than Y-doped SrTiO_3 , because the atomic radius of La is closer to Sr [16], and therefore it is widely studied [17].

Marina and Canfield et al. [18] prepared $\text{La}_x\text{Sr}_{1-x}\text{TiO}_3$ sintered at $1650 \text{ }^\circ\text{C}$ under a 2% hydrogen condition, and reported its metal-like behavior and its high conductivity of $400\text{--}5000 \text{ S cm}^{-1}$ in both air and hydrogen. Such high conductivity has suggested that La-doped SrTiO_3 is a potential component of SOFCs. They also found that La content had a significant influence on the conductivity of $\text{La}_x\text{Sr}_{1-x}\text{TiO}_3$ [18]. With an increase in La content, the conductivity increased under a reducing atmosphere and reached a very high value of $3.0 \times 10^2 \text{ S cm}^{-1}$ at $1000 \text{ }^\circ\text{C}$ when $x=0.4$ [19, 20]. It has been reported that the maximum solubility level is 40 at.% for La in $\text{La}_x\text{Sr}_{1-x}\text{TiO}_3$ without distortion of the strontium titanate structure [18].

In recent years, research on the electrical properties of LST composite anodes has increased substantially [21–24]. Although LST delivers good electronic conductivity, its ionic conductivity is low and this needs to be compensated for by adding $\text{Y}_{0.2}\text{Ce}_{0.8}\text{O}_{2-8}$, $\text{Gd}_{0.1}\text{Ce}_{0.9}\text{O}_{1.95}$, YSZ, or other electrolyte materials [25–28]. Koo et al. [29] synthesized a $\text{La}_{0.2}\text{Sr}_{0.8}\text{TiO}_3\text{--Gd}_{0.1}\text{Ce}_{0.9}\text{O}_{1.95}$ (LST-GDC) composite anode material using the solid-state reaction method in a reducing atmosphere (5% $\text{H}_2\text{--}95\%$ Ar). The conductivity of the LST-GDC composite anode material in H_2 was about 37 S cm^{-1} at $800 \text{ }^\circ\text{C}$. The maximum power density of 25 mW cm^{-2} at $800 \text{ }^\circ\text{C}$ in CH_4 fuel was obtained with the LST-GDC anode. Luo et al. [30] prepared an active $\text{La}_{0.4}\text{Sr}_{0.6}\text{TiO}_{3\pm\delta}\text{:Y}_{0.2}\text{Ce}_{0.8}\text{O}_{1.9}$ (50:50) (LST-YDC) composite anode using materials

manufactured using a modified citrate-nitrate gel combustion method. The polarization resistance of the LST-YDC composite anode was $12 \text{ } \Omega \text{ cm}^2$, and the maximum energy density was 102 mW cm^{-2} at $850 \text{ }^\circ\text{C}$ in syngas (40% $\text{H}_2\text{--}60\%$ CO).

As stated, LST materials have generally been synthesized in a reducing atmosphere. Despite the good conductivity achieved by high-temperature sintering under a reducing atmosphere, it is not recommended, as it increases system complexity and cost. As an anode material, it needs to be thermally and mechanically stable. In some cases, it must be stable over a wide range of oxygen partial pressure levels in a reducing atmosphere and under oxidizing conditions during system thermal cycling. For this reason, much attention is currently being given to developing novel SOFC anode materials that are capable of delivering the required electrochemical performance, but with less demanding fabrication conditions. The air-sintered samples exhibited unique advantages over the application on SOFCs, as these are more stable under redox cycling conditions than the sample sintered in a reducing atmosphere [18]. Hashimoto et al. [31] demonstrated that the conductivity of $\text{La}_{0.3}\text{Sr}_{0.7}\text{TiO}_3$ is less affected by the atmosphere, e.g., air or steamed H_2/N_2 or 9% H_2/N_2 , over a wide temperature range (800 to $1300 \text{ }^\circ\text{C}$) than that of $\text{La}_{0.1}\text{Sr}_{0.9}\text{TiO}_3$. This demonstrates that $\text{La}_{0.4}\text{Sr}_{0.6}\text{TiO}_3$ would probably exhibit good conductivity over a wide range of oxygen partial pressure levels, regardless of the fabrication process [31].

Lattice oxygen increases with an increasing La content. Also, increasing the La doping level leads to an increasing concentration of n-type charge carriers and, therefore, an increase in conductivity [18]. In general, the key factors, including temperature, oxygen partial pressure, and dopant amount, have been investigated to adjust the conductivity. LST materials with higher lanthanum doping levels show better conductivity over a wide range of oxygen partial pressure levels.

A three-electrode model is often applied when investigating electrode performance [32]. In the three-electrode system, the electrode to be studied can be separated from the effect of other electrodes, and it will then not be influenced by the other electrodes. Some three-electrode systems have been developed to investigate electrode overpotential [33]. To date, the cathode of the LSM-YSZ electrode has been studied most often using the three-electrode mode [34]. The cathode atmosphere is usually the same as the reference electrode and counter; therefore, it is a simple process to locate the position of the counter and reference electrodes.

Most of the research done on SOFCs using LST anodes has been focused on whole-cell performance, while little attention has been paid to the anode overpotential of titanate in a three-electrode mode [35]. The $\text{La}_{0.3}\text{Y}_{0.1}\text{Sr}_{0.4}\text{TiO}_{3-6}$ [36] and $\text{La}_{0.2}\text{Sr}_{0.8}\text{TiO}_3\text{--GDC}$ [35] composites have been

investigated using a three-electrode configuration, but not many details were provided in the research reports. Based on the literature survey done, it would be worth the effort to simplify the preparation condition of La-doped SrTiO₃ and develop a characterization method for the electrochemical performance of the LST anode.

In this work, La-doped SrTiO₃ powder was synthesized using a solid-state reaction method and calcined in air, rather than a reducing atmosphere. In order to enhance electrocatalytic performance, YSZ was added, to form the LST–YSZ composite anode. Similarly, air was used for sintering the LST–YSZ composite anode. The electrochemical impedance spectroscopy and overpotential were investigated in a three-electrode mode. According to San Ping Jiang's report, a cell structure with a symmetrical electrode geometry system and the reference electrode at the side of the counter electrode is suitable for use in the planar cell test [37]. In this study, it was a requirement that a real working condition was simulated; therefore, the working electrode of LST–YSZ was exposed to reducing conditions and the counter electrode and reference electrode were exposed to air. The electrochemical performance and long-term durability of the LST–YSZ composite anode in a sulfur-containing fuel (in a 10,000 ppm H₂S–H₂ feed) were also tested.

2 Experimental

2.1 Preparation of LST–YSZ composite electrode

The perovskite powders La_{0.4}Sr_{0.6}TiO₃ were prepared from La₂O₃, TiO₂, and SrCO₃ (analytical grade; all obtained from Sigma–Aldrich) by means of the solid-state reaction. The powders were mixed and ball-milled for 24 h with propanol. The mixture was then calcined at different temperatures for 20 h at 1350 °C in air. The ink of the LST–YSZ (TZ-8Y, Tosoh, Japan) composite electrode was prepared by mixing the as-prepared LST and commercial YSZ powders with PVB (Butvar B-76, Eastman) and isopropanol (95%, Alfa). The content of YSZ in the composite electrode was 30 wt%, 40 wt%, 50 wt%, 60 wt%, or 70 wt%.

2.2 Three-electrode mode

Electrolyte substrates were prepared from YSZ powders by dry-pressing and then sintered at 1600 °C for 4 h. The diameter and thickness of the YSZ pellets were ~ 18 mm and ~ 1 mm, respectively. The surface of the YSZ discs was ground using sandpaper, to increase the roughness and the contact area between the electrode and the YSZ electrolyte.

The LST–YSZ composite ink was painted onto the YSZ pellets with a brush, and sintered at 1100 °C, 1200 °C, 1300 °C, 1350 °C, and 1400 °C. After sintering, the thickness

of the anode was about 20 μm, and the surface area of the working electrode was 0.5 cm². The platinum paste (Ferro Corporation, USA) was coated on the other side of the YSZ electrolyte and then calcined at 800 °C for 1 h. This served as the counter and reference electrodes. The counter electrode was symmetrical to the working electrode, and a reference electrode was painted as a ring around the counter electrode. The distance between the counter and reference electrodes was about 4 mm. Pt mesh was used as a current collector for both working and counter electrodes, and two Pt wires were spot-welded to the current collector as current and voltage probes separately. The cell configuration is shown in Fig. 1.

The LST–YSZ anode was sealed into an alumina tube with a sealant (552 Aremco). The anode was supplied with saturated hydrogen when the cell was heated up at a heating rate of 5 °C/min. All tests were measured in a steady state at 1000 °C after two hours, and tested at each temperature level at 50 °C intervals. The electrochemical impedance spectra were measured in a three-electrode mode, with the fuel electrode (working electrode) fed with 97% H₂/3% H₂O. The counter electrode and Pt reference electrode were exposed to ambient air. The impedance spectra were recorded in the frequency range 1 MHz to 0.01 Hz with an Ac amplitude of 10 mA using an Autolab station (Netherlands). The electrochemical curves of current density and voltage were recorded as well.

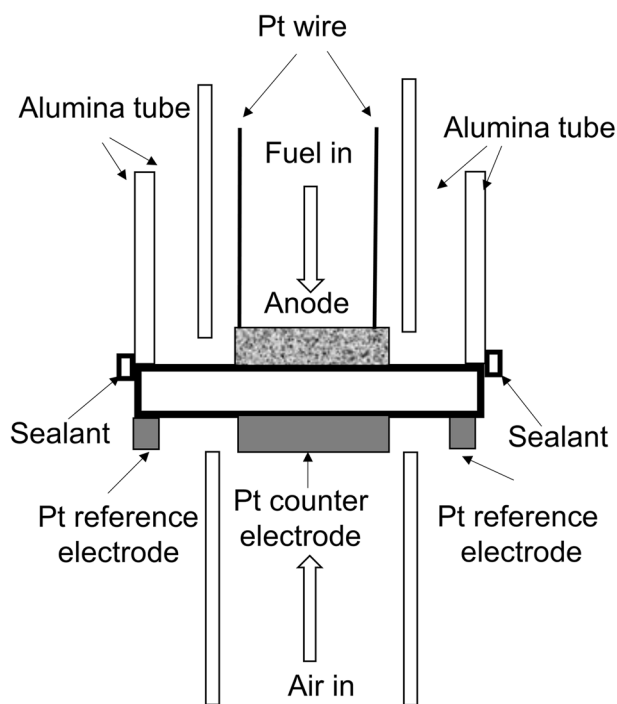


Fig. 1 Schematic diagram of cell configuration

The polarization potential (E_{cathode}) of the LST–YSZ composite electrode was measured against the Pt reference electrode. The ohmic resistance R_{Ω} of the electrode and electrolyte was measured from the high-frequency intercept at the x -axis. The electrode interface polarization resistance R_p was obtained from the difference between the high-frequency and low-frequency intercepts on the impedance spectra at the x -axis. Thus, the anode overpotential (η) could be obtained from the electrode potential of $E_{\text{electrode}}$ and the ohmic resistance of R_{Ω} by means of the following equation.

$$\eta = E_{\text{electrode}} - jR_{\Omega} \quad (1)$$

where j is the current density.

2.3 Single cell

A YSZ (Tosoh, TZ-8Y, Japan) electrolyte with a $\sim 400 \mu\text{m}$ thickness was used for a single-cell test in a two-electrode mode. The electrochemical measurements were performed on the composite anode in 97% $\text{H}_2/3\% \text{H}_2\text{O}$, or a 10,000 ppm $\text{H}_2\text{S}-\text{H}_2$, using a temperature range of 850–1000 °C. The fuel was fed into the anode at a flow rate of 50 ml min^{-1} , while ambient air was applied in the cathode. The electrochemical impedance spectra were measured using an Autolab station (Netherlands) with an applied frequency of $0.01\text{--}10^6$ Hz and an ac amplitude of 10 mV. Electrochemical curves were recorded as well.

2.4 Other characteristics

The LST phase sintered at 1400 °C (JCPDS No. 79-0188) was characterized by X-ray diffraction (Philips, Netherlands). (See Fig. 2.) Scanning electron microscopy (SEM, JOEL 350, Japan) and X-ray energy dispersion spectroscopy (Bruker, Germany) were employed to observe the microstructure of the LST–YSZ composite anode and test the element distribution. SEM images of the as-prepared LST powders sintered at 1350 °C and Tosoh Powders were tested with scanning electron microscopy (VEGA 3SBU, TESCAN, Czech). The particle size distribution was characterized with a Malvern laser particle size analyzer (Mastersizer 3000).

3 Results and discussion

3.1 Sintering temperature of the composite anode

3.1.1 Polarization resistance

First, the impedance spectra of the LST–YSZ (60 wt% YSZ) composite anode at different sintering temperatures were measured. The results are shown in Figs. S1, S2, S3, S4,

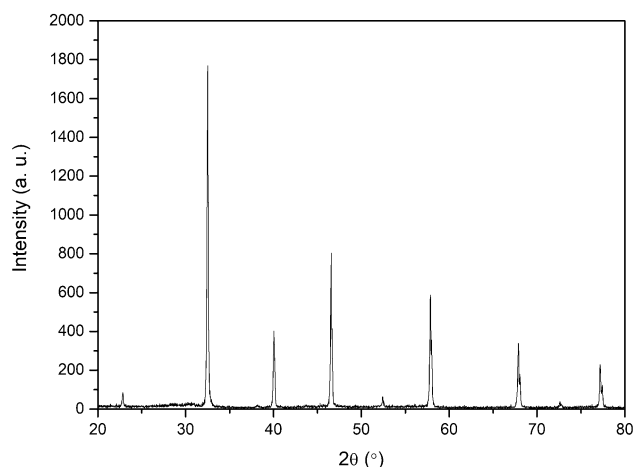


Fig. 2 XRD patterns of the as-prepared $\text{La}_{0.4}\text{Sr}_{0.6}\text{TiO}_3$

and S5 for the anode sintered at 1100 °C, 1200 °C, 1300 °C, 1350 °C, and 1400 °C. Each electrode was tested at four temperatures: 1000 °C; 950 °C; 900 °C; 850 °C.

Figure 3 shows a typical impedance response of the LST–YSZ composite anode tested at 850 °C. The intercept of impedance spectra at high frequencies on the real axis is the ohmic resistance (R_{Ω}) between the anode and the reference electrode. The anode sintered at 1100 °C exhibited the highest ohmic resistance (R_{Ω}) of all the samples—almost six times more than the one sintered at 1350 °C. The arc between low frequencies and high frequencies is attributed to the anode polarization resistance (R_p).

With hydrogen oxidation at 850 °C, the electrode polarization resistance is 3.37, 1.31, 1.07, 0.66, and $2.02 \Omega \text{ cm}^2$ for the LST–YSZ composite anode sintered at 1100, 1200, 1300, 1350 and 1400 °C, respectively. (See Fig. 3a.) The impedance spectra show that the electrochemical behavior of the LST–YSZ composite anode varies a great deal with variation in the anode sintering temperature. The lowest R_p was obtained when the anode was sintered at 1350 °C. With a low sintering temperature of 1100 °C, R_p is $3.37 \Omega \text{ cm}^2$, which is much higher than the $0.66 \Omega \text{ cm}^2$ for the anode sintered at 1350 °C.

Considering the thermal history of LST powders, the sintering behavior of the LST–YSZ composite anode probably relates to the pretreatment of the LST and YSZ powders. Generally, 1100 °C is not a high enough temperature for sufficient shrinkage of YSZ and LST, which may be the main reason why remarkably high resistance of the anode was generated under this temperature. That is, the connectivity of LST to LST and YSZ to YSZ is poor. Therefore, it is required to increase the temperature to be above 1100 °C. There is no significant difference between the impedance spectra obtained at 1200 and 1300 °C at high frequency. However, the resistance value at a low

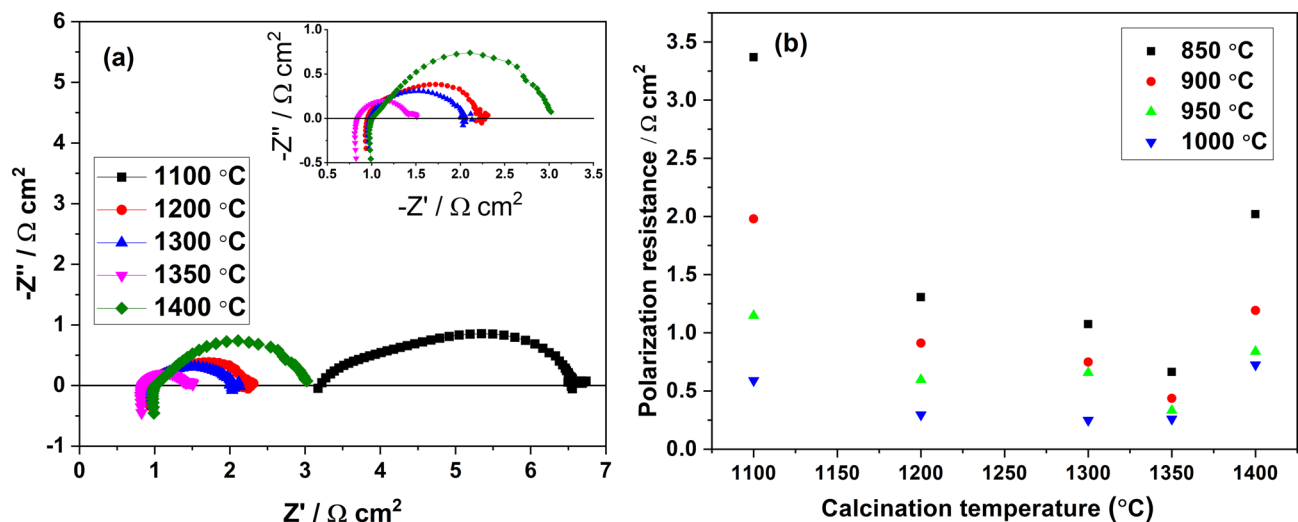


Fig. 3 Effect of the anode calcination temperature on the electrode polarization resistance. **a** Selected electrochemical impedance spectra of LST–YSZ composite anode calcined at different temperatures

frequency of $1.31 \Omega \text{ cm}^2$ of the sample sintered at $1300 \text{ }^\circ\text{C}$, which is probably caused by the sintering initiation of YSZ at that temperature. Despite a further decrease in polarization resistance of the anode sintered at $1300 \text{ }^\circ\text{C}$, the total resistance levels, including the ohmic contact resistance and electrode interfacial resistance, of the anode sintered at $1300 \text{ }^\circ\text{C}$ are still relatively high compared with the anode sintered at $1350 \text{ }^\circ\text{C}$. When the sintering temperature is increased to $1350 \text{ }^\circ\text{C}$, the shrinkage of YSZ and LST may lead to a valid connection between these two phases, which enlarges the triple-phase boundary for electrochemical reaction. However, a further increase in the sintering temperature to $1400 \text{ }^\circ\text{C}$ has no positive effect—in fact, it arouses deadly degradation in the performance of the LST–YSZ electrode, which probably results from the densification of YSZ. There is a suitable sintering temperature for the anode in order to achieve a low polarization resistance. The polarization resistance is a comprehensive result of the microstructure and composition of the electrode. An appropriate porosity and content of each composition are required [38]. As far as the shrinkage properties are concerned, it is affected by the sinterability and content of each composition in the anode [39]. It is reported that the shrinkage of YSZ is 26%, which is close to NiO in the NiO–YSZ electrode. The polarization resistance in this study is not quantified by the shrinkage yet, but there are some effects that could be seen by the size difference of YSZ and LST [40]. Appropriate particle size and a suitable ratio of each composition are crucial to the conductivity of the cell [7]. The resistance of the cell is the result of the

(measured at $850 \text{ }^\circ\text{C}$); **b** Electrode polarization resistances of the LST–YSZ composite tested at different temperatures

distribution of pores, LST and YSZ. It seems that $1350 \text{ }^\circ\text{C}$ is an optimal sintering temperature in this study.

In this case, the easiest path of electron transportation is possibly being prevented by YSZ. Therefore, the cell shows high electrode interfacial polarization. The value of $0.66 \Omega \text{ cm}^2$ at $850 \text{ }^\circ\text{C}$ is significantly lower than the reported data of $2.6 \Omega \text{ cm}^2$ with a SYT (Y-doped SrTiO_3)–YSZ composite anode sintered in $\text{Ar}/4\%\text{H}_2$ tested at $800 \text{ }^\circ\text{C}$, but is comparable to the data of $0.49 \Omega \text{ cm}^2$ of the anode sintered in $\text{Ar}/4\%\text{H}_2$ and tested in wet $\text{Ar}/5\%\text{H}_2$ at the same temperature [12]. The polarization resistance of the cell is comparable with that of the YSZ scaffold impregnated with 45 wt% a $\text{La}_{0.3}\text{Sr}_{0.7}\text{TiO}_3$ electrode containing 0.5 wt% Pd and 5 wt% Ceria [26].

The value of R_p of the reaction on the LST–YSZ composite anode as a function of the anode sintering temperature is plotted in Fig. 3b. The sintering temperature has a significant effect on the impedance response at a low frequency, which is clearly shown in Fig. 3a. When considering the total range of the testing temperatures, it is seen that R_p decreases with the sintering temperature of the anode, and reaches the lowest level when the sintering temperature is $1350 \text{ }^\circ\text{C}$, but increases when a higher sintering temperature is applied. Especially at a lower testing temperature, the influence of sintering temperature on the anode performance is more prominent. Under a testing temperature of $850 \text{ }^\circ\text{C}$, the R_p of the anode is sintered at $1100 \text{ }^\circ\text{C}$ —five times more than the anode sintered at $1350 \text{ }^\circ\text{C}$; however, a smaller effect of the sintering temperature on the R_p was found when the anode was tested at a high temperature of $1000 \text{ }^\circ\text{C}$.

3.1.2 Anode overpotential

The anode potential of the composite electrode sintered at different temperatures was tested, and the results are shown in Fig. 4. Figure 4a shows the anode polarization characteristics of the sample tested at 850 °C, using Pt as a reference electrode. Figure 4a is obtained by linear sweeps from open-circuit potential to a value of 0.9 vs. open-circuit voltage. The anode potential is the voltage between the anode and the Pt reference electrode. The current density is tested between the working electrode(anode) and the Pt counter electrode. The anode overpotentials are calculated using Eq. (1) as shown in Fig. 4b. The electrode potential ($E_{\text{electrode}}$) is obtained by subtracting the voltage value of individual data points from the open-circuit voltage in Fig. 4a. The ohmic resistance R_{Ω} is estimated from the high-frequency intercept of the impedance spectra at the x -axis. The current density is the value at each anode potential in Fig. 4a. Therefore, the anode overpotential results from extracting ac ohmic drop ($j \times R_{\Omega}$) from the electrode potential ($E_{\text{electrode}}$). There is a tiny potential between the counter electrode and the reference electrode. The value is usually very small (a few microvolts) and can be ignored. There are a few configurations with the different electrode and reference positions considering the polarization performance using the three-electrode mode. The arrangement of the overpotential test in this study with the working and counter electrodes in the center and the reference at the side is a suitable selection as compared to the other reference configurations since there is no risk of a build-up of water or inactive electrolyte regions [37]. A thick electrolyte about 1 mm is used in this study and ohmic resistance is the main loss. The contribution of

ohmic resistance at a higher current density is much bigger than the polarization resistance from the electrode. We can see that the anode overpotential is slightly bigger than the anode potential. Therefore, except for the electrode overpotential, ohmic resistance is another parameter needed to be considered in whole-cell fabrication. The overpotential of the anode sintered at 1100 °C is very high, with a value of 0.36 V at a current density of 0.1 A cm⁻² when it was tested at 850 °C. The overpotential decreases with an increase in the anode sintering temperature.

For the anode sintered at 1400, 1350, 1300, and 1200 °C, the overpotentials produced with the same conditions are 0.21, 0.06, 0.11, 0.09, and 0.36 V, respectively. Therefore, we can see that the lowest overpotential is obtained with the sample sintered at 1350 °C, which is consistent with the anode polarization resistance results shown in Fig. 3 [15]. These results show that the anode sintering temperature plays a key role in anode polarization.

3.1.3 Microstructure observation

The microstructures of the LST–YSZ composite anodes sintered at different temperatures after electrochemical testing are observed. The cross-sections are shown in Fig. 5. When the anode was sintered at 1200 °C, no valid sintering process took place. Therefore, LST and YSZ powders aggregate in a dispersed manner. When the sintering temperature increased to 1300 °C, the LST and YSZ powders began to shrink and started to connect, while also producing some pores.

The shrinkage and connectivity of LST and YSZ with a 1350 °C sintering temperature produced adequate porosity for gas transportation. In this case, the average grain size

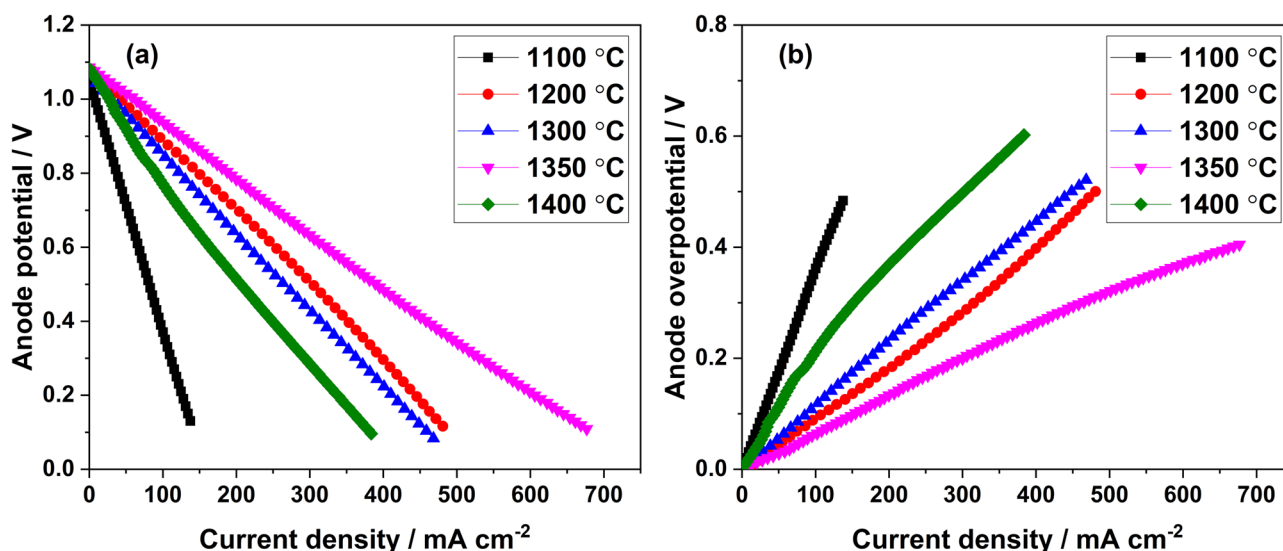


Fig. 4 Electrochemical polarization characteristics of the LST–YSZ composite anode calcined at different temperatures. **a** Anode potential; **b** Anode overpotential

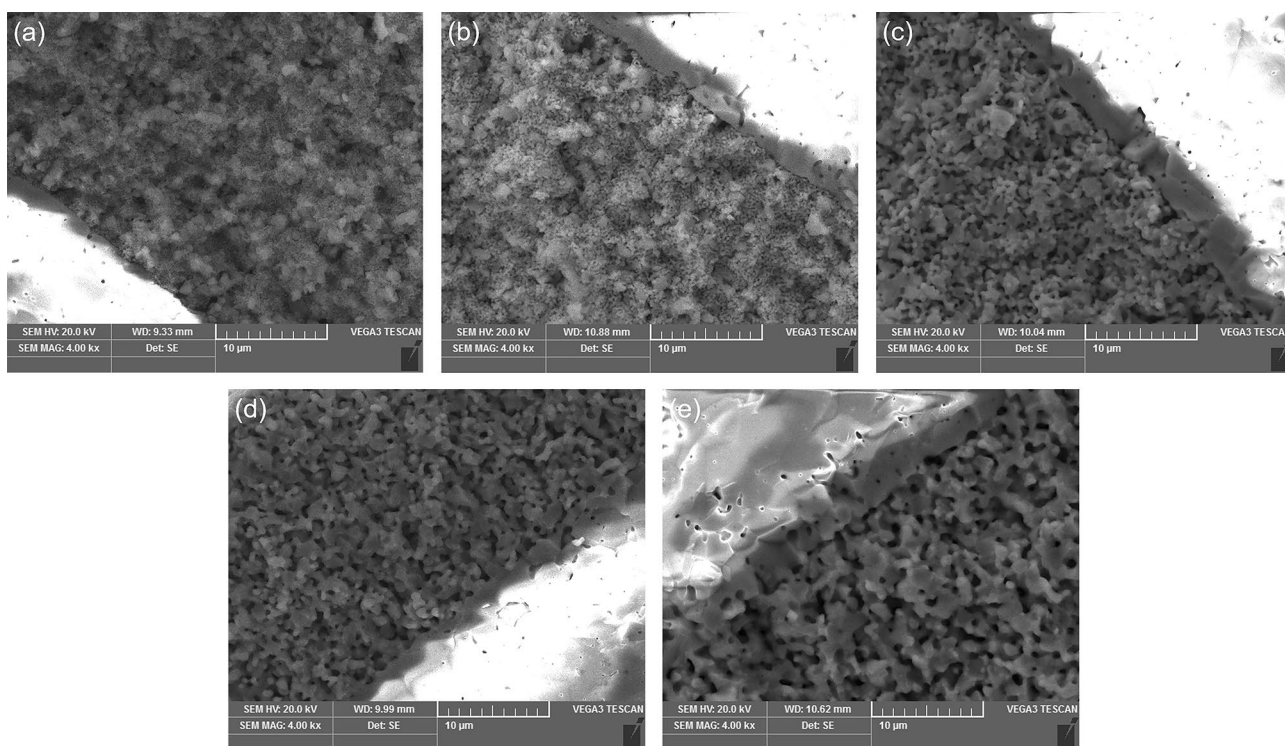


Fig. 5 Microstructure of the LST–YSZ (60 wt%) composite anode sintered at different temperatures. **a** 1100 °C; **b** 1200 °C; **c** 1300 °C; **d** 1350 °C; **e** 1400 °C

of the anode was about 1 μm . The highest performance of LST–YSZ sintered was obtained at 1350 °C, which implies that the electrode has a proper microstructure, uniform porosity, and grain size. Furthermore, the LST–YSZ composite anode shows reasonable contact with the YSZ electrolyte. YSZ could prevent the electron transportation of LST as the conductivity is dependent on the contact of LST in the LST–YSZ composite electrode, which is similar to the results reported by Matsushima [39]. The polarization resistance at 1400 °C is higher than those of 1200, 1300, and 1350 °C in this study. The increased value is possibly due to the densification of YSZ as the YSZ powder has fine particle sizes. Exaggerated growth of grain was observed when a 1400 °C sintering temperature was used. It is also suggested that it would be beneficial to have close sintering ability and grain growth of each composition in the composite electrode. Therefore, the transportation pathway may be blocked due to this adverse effect, which resulted in high anode polarization resistance. (See Fig. 3.)

Microstructure observation is one of the most effective means of estimating electrode performance. The SEM images provided here prove the polarization resistance discrepancy sintered at different temperatures and the overpotential results, as detailed in the above sections. The image and XRD pattern of the composite electrode sintered at 1350 °C before and after electrochemical tests are shown in Fig. 6.

It can be seen that there are fewer pores (Fig. 6a) before electrochemical testing and more pores after testing (Fig. 6c). The XRD patterns show the peaks YSZ and LST (Fig. 6b, d).

3.1.4 Element analysis of the cross-section

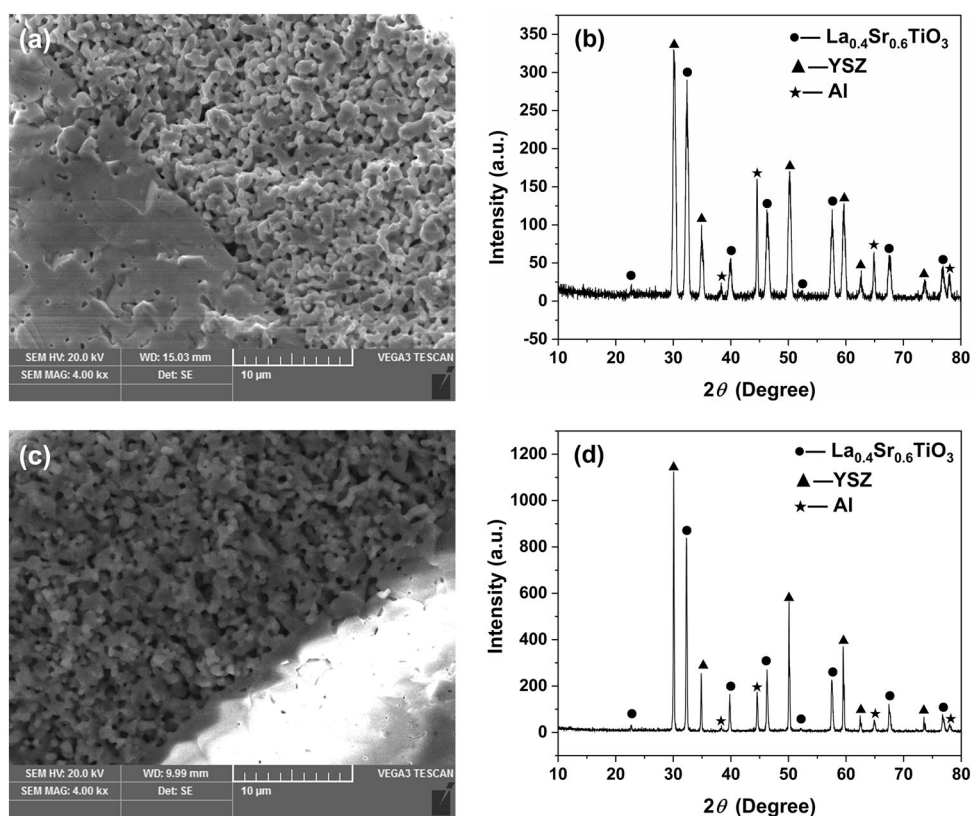
EDX linear scanning analysis results of the cross-section of the YSZ/LST–YSZ interface are shown in Fig. 7. Images of the LST–YSZ microstructure and distribution of La, Sr, Ti, Zr, Y, and O in the interface are shown in Fig. 7a–f. There was no noticeable element migration between the LST–YSZ composite anode and the YSZ electrolyte when the anode was sintered at 1350 °C. These results clearly show that the LST is compatible with the YSZ electrolyte.

A clear boundary is seen between the LST–YSZ composite electrode and the YSZ pellet. No significant diffusion is seen between the LST and YSZ pellet. This indicates that no reaction between LST and YSZ occurred, even though a high sintering temperature of 1550 °C was used [14].

3.2 YSZ content in the composite anode

The anode requires both an ionically and electronically conductive component. Impedance spectra, anode I–V plot, and SEM were used to investigate the resistance, overpotential, and microstructure of the LST–YSZ composite anode.

Fig. 6 SEM images and XRD patterns of the LST–YSZ (60 wt%) composite anode sintered at 1350 °C. **a** SEM images before test; **b** XRD patterns before test; **c** SEM images after test (the same image as Fig. 5d); **d** XRD patterns after test



The results are shown in Fig. 8. When a low YSZ content is applied to the LST–YSZ composite anode, the polarization resistance of the anode is very high. (See Fig. 8a.) An increase in the YSZ content above 50 wt% results in a decrease in the polarization resistance. The impedance spectra show that the lowest polarization resistance ($0.26 \Omega \text{ cm}^2$) is obtained on the cell with 60 wt% YSZ. Similar to resistance results, the anode overpotential is low when a large amount of YSZ content is used. (See Fig. 8b) The data indicate that there is a continuous decrease in polarization resistance with an increase in the YSZ content. The polarization resistance of the LST–YSZ composite anode depends on the YSZ content. It is well known that insufficient ionic conductivity is one of the disadvantages of titanate [41]. It has been reported that CeO_2 could enhance the ionic conductivity of $\text{La}_{0.2}\text{Sr}_{0.8}\text{TiO}_3$ and, in this study, the composite $\text{La}_{0.2}\text{Sr}_{0.8}\text{TiO}_3\text{--CeO}_2$ electrode exhibited the minimum polarization resistance, i.e., $1.2 \Omega \text{ cm}^2$ at 900 °C [42]. Here, YSZ provides ionic conductivity, and LST provides mostly electronic conductivity.

Figure 9 shows the SEM images of the fractured cross-sections of the LST–YSZ composite anodes with different YSZ amounts. Figures 9a–e are images of the electrodes with 30 wt%, 40 wt%, 50 wt%, 60 wt%, and 70 wt% YSZ. It can be seen that the pore size of the electrode with a low YSZ content is quite large, i.e., about $5 \mu\text{m}$. With an increase in the YSZ content in the LST–YSZ composite anode, the

pore size becomes smaller. Furthermore, the distribution of LST, YSZ and pores, is uniform. This further verifies the above result of resistance and overpotential.

In the next studies, hydrocarbon fuel and sulfur fuel were investigated; therefore, we used 60 wt% YSZ for the following experiment.

SEM images of LST, Tosoh, and particle size distributions are shown in Fig. S6. The particle sizes of LST are significantly different from those of Tosoh (Fig. S7), which can be seen in the SEM images of the starting powders of LST and Tosoh YSZ. (See Figs. S6a, S6b.) However, little difference is found in the particle size distribution when testing on the Malvern laser particle size analyzer. It can be seen that the particle sizes of LST (Fig. S7a) and Tosoh YSZ (Fig. S7b) are much bigger than those revealed by SEM images. The difference in particle size of these two powders could be because of the agglomeration of fine Tosoh YSZ powders. At a relatively low temperature (e.g., 1100 °C), the grain size of the Tosoh powders is fine, as seen in Fig. 5a. With an increase in temperature, the grain size of Tosoh grows, but the growth of LST grain size is not significant. Therefore, a significant difference in grain size is observed for the composite electrodes sintered at 1100 °C, 1200 °C (Fig. 5b), 1300 °C (Fig. 5c), 1350 °C (Fig. 5d), and 1400 °C (Fig. 5e).

An optimized ratio of YSZ located around 60 wt% YSZ can be interpreted using the percolation theory. Kusy developed an equation for percolation by investigating

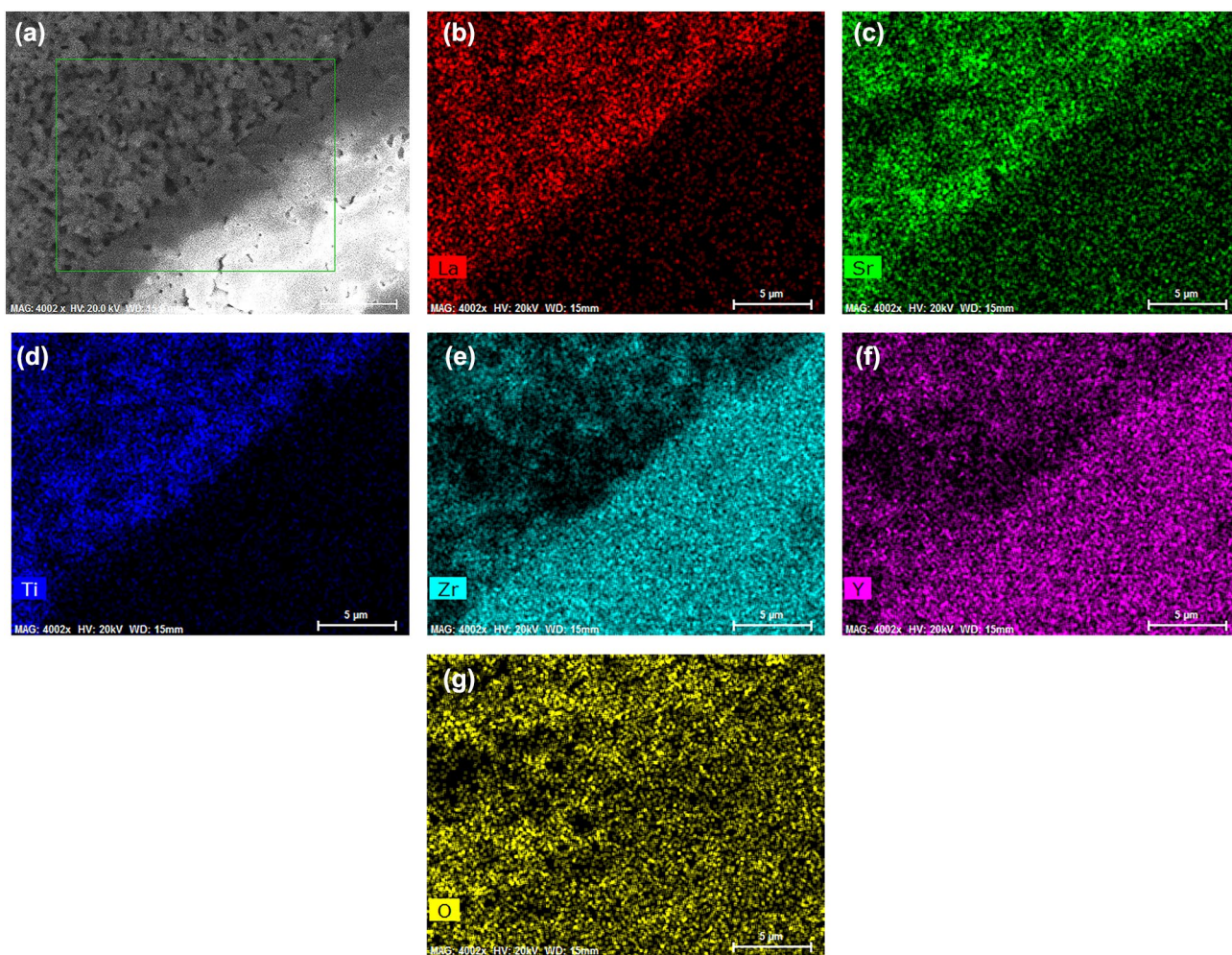


Fig. 7 SEM image combined with the energy dispersive X-ray (EDX) spectra at the interface of the anode and electrolyte. **a** SEM image; **b** La; **c** Sr; **d** Ti; **e** Zr; **f** Y; **g** O Zr(red), Y(yellow), Ti(green), Sr(cyan), O(blue), La(magenta)

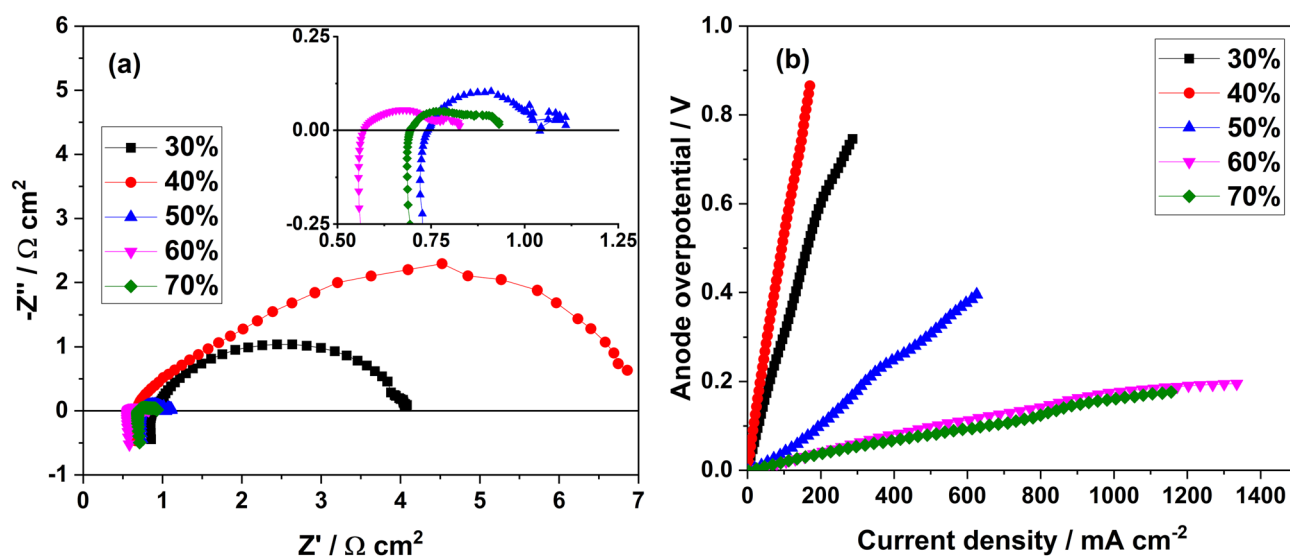


Fig. 8 Electrochemical performance of the cell with various YSZ content. **a** EIS of LST-YSZ with different LST-YSZ weight ratios of anode in $\text{H}_2(97\%)/\text{H}_2\text{O}(3\%)$ fuel testing at 900°C ; **b** Anode overpotential (Vs Pt reference electrode) in $\text{H}_2(97\%)/\text{H}_2\text{O}(3\%)$ fuel tested at 900°C

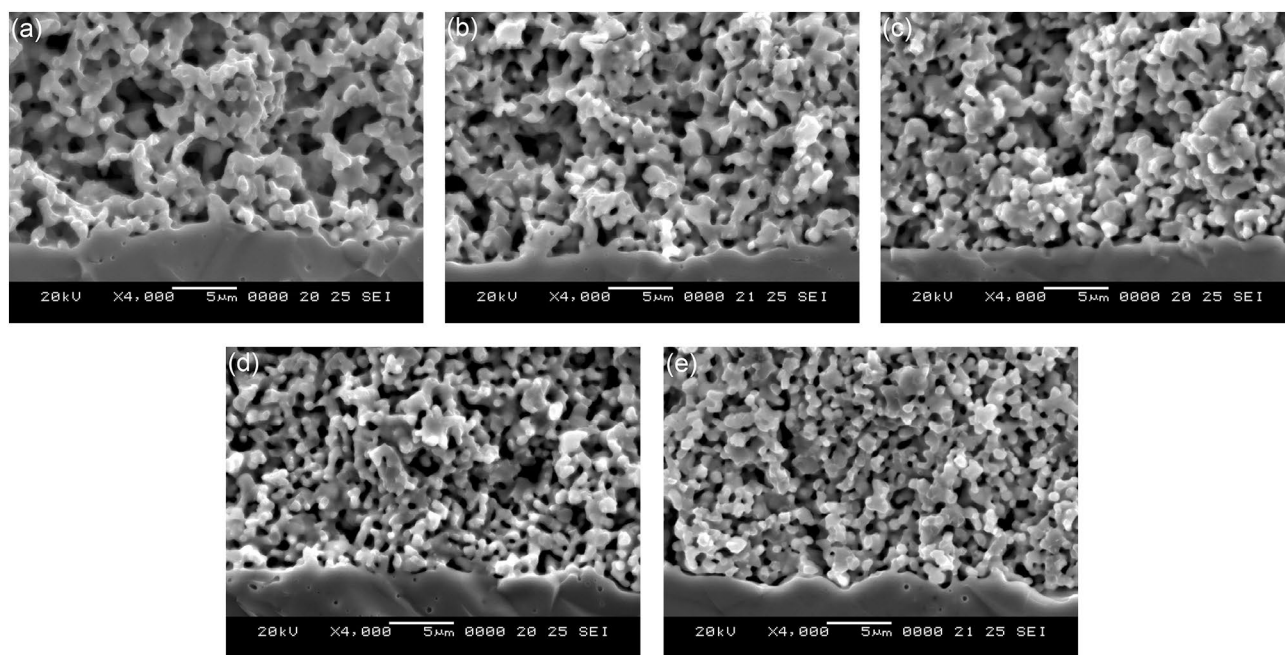


Fig. 9 SEM images of the LST–YSZ composite anode with various YSZ content. **a** 30%; **b** 40%; **c** 50%; **d** 60%; **e** 70%

the effect of particle size ratio on percolation in mixtures of metals and polymers [43].

$$V_c = 100 \left[1 + \left(\frac{\phi}{4X_c} \right) \left(\frac{R_p}{R_m} \right) \right]^{-1}, \quad (2)$$

where X_c 0.42; ϕ 1.27 for the cubic lattice; V_c percolation limit; R_p radius of the polymer particle; R_m radius of the metal particle.

The value of the percolation limit is calculated using Eq. (2). The grain sizes of YSZ and LST are 2 and 1 μm , as estimated from the SEM images shown in Fig. 9. The connectivity of YSZ can be calculated according to Eq. (2) and the value is 39.81 vol%. The densities of LST and YSZ are 5.686 and 5.9 g/cm^3 , respectively. When 40 wt% YSZ is added to the LST–YSZ composite electrode, the volume percentage of the YSZ amount is 39.12 vol%. This calculation verifies that big polarization resistance levels are obtained on the LST–YSZ composite with 30 wt% and 40 wt% YSZ. This means that the YSZ network is not formed up to 40 wt% of YSZ, and YSZ powder is isolated by LST powder. The isolated YSZ does not exhibit electrochemical activity; only connected YSZ has electrochemical activity [44]. Above 50 wt%, the added YSZ powder developed connectivity, so better electrochemical performance is obtained on the LST–YSZ electrode with a higher content of YSZ.

3.3 Sulfur tolerance

It is of great interest to employ the LST anode in SOFC operating in H_2S -containing fuels, as an alternative anode catalyst. The cell performance in hydrogen and H_2S - H_2 is shown in Fig. 10. In this study, a high concentration of H_2S was applied to test the limitation of sulfur tolerance. The investigation done by Mukundan et al. [45] showed no degradation when the LST anode was exposed to up to 5000 ppm of H_2S in hydrogen fuel. However, nickel could be deactivated or fail at a few ppm levels of H_2S [46].

A 50 ppm H_2S caused a sharp drop in cell performance of Ni–YSZ within the first few minutes of exposure [47]. The LST–YSZ composite anode shows high electrochemical catalysis for the fuel containing H_2S at a lower temperature. For example, the maximum power density of the cell at 850 $^\circ\text{C}$ with hydrogen fuel is 117 mW cm^{-2} (Fig. 10a). At the same temperature, in the presence of 10,000 ppm H_2S in hydrogen, the maximum power density of the cell increases to 132 mW cm^{-2} . (See Fig. 10b.) The cell performance could be further improved by using a thinner electrolyte (400 μm in the present study), due to possible lower ohmic resistance.

In this study, the behavior of the LST–YSZ composite anode was investigated in the presence of 10,000 ppm H_2S and H_2 mixed gas fuel. When the LST–YSZ anode was exposed to 10,000 ppm H_2S under similar conditions, the fuel cell performance showed significant improvement of

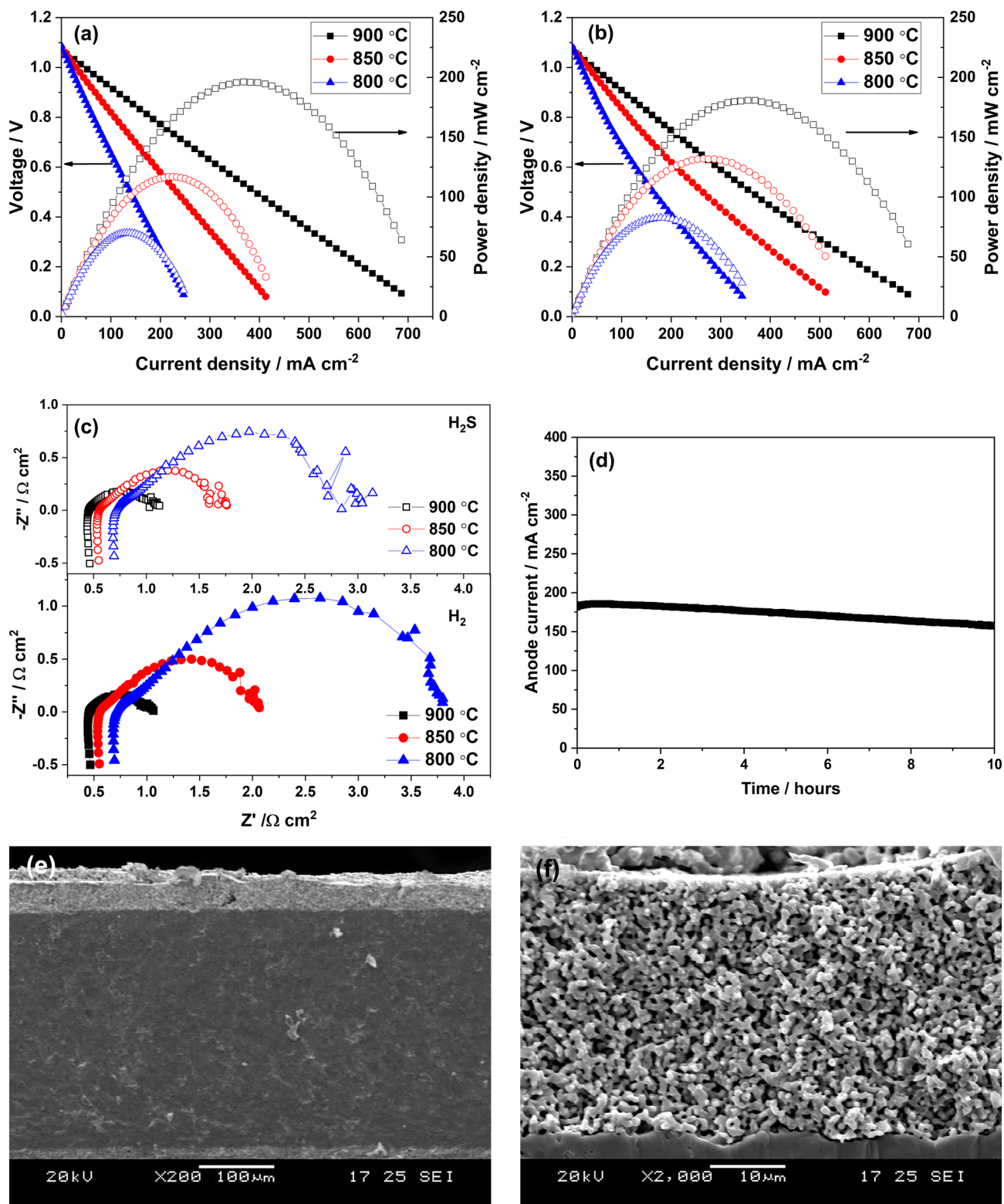


Fig. 10 Fuel cell performance of a single cell with an LST–YSZ anode, and a YSZ electrolyte and a (La_{0.8}Sr_{0.2})_{0.9}MnO_{3–δ}–YSZ cathode tested in H₂ and H₂S-containing H₂. **a** Power output of the cell in

H₂; **b** Power output of the cell in 10,000 ppm H₂S–H₂; **c** Impedance spectra of the cell; **d** Durability of the cell in 10,000 ppm H₂S–H₂

the impedance spectra under open-circuit conditions. For instance, the resistance of the LST-based cell in hydrogen at 800 °C is $\sim 3.04 \Omega \text{ cm}^2$ (Fig. 10c), while the resistance is only $\sim 2.32 \Omega \text{ cm}^2$ when the same anode is exposed to 10,000 ppm H_2S . (See Fig. 10c.) This superior polarization resistance is much smaller than the resistance of $7 \Omega \text{ cm}^2$ of the impregnated $\text{La}_{0.4}\text{Ce}_{0.6}\text{O}_{1.8}\text{--}\text{La}_{0.4}\text{Sr}_{0.6}\text{TiO}_3$ in 5000 ppm $\text{H}_2\text{S}\text{--}\text{H}_2$ tested at 800 °C [48]. A high concentration of sulfur is used in this study. Therefore, sulfur could be fuel. Sulfur could be dissociated on the surface of LST catalysts. The association of sulfur could promote catalytically by changing the reaction process in a favorable direction [49]. The actual maximum power density of the cell in sulfur-containing fuel is smaller than that in hydrogen. The resistance and cell output give contradictory results. It demonstrates that chemical reactions and electrochemical reactions could be significantly different in the presence of sulfur. A high concentration of 10,000 ppm H_2S is used in this study. There are not many reports about this high level of H_2S [50]. The extremely high sulfur could be the main reason that causes a different behavior of resistance. Another possibility is the test procedure. The cell performance is tested in hydrogen first and then tested in 10,000 ppm $\text{H}_2\text{S}\text{--}\text{H}_2$ and then switch back to hydrogen. The discontinuous supply of sulfur makes the dissociation process changed so that a smaller resistance of sulfur-fueled cells is found.

Rath et al. [51] investigated the influence of various volume ratios of $\text{La}_{0.2}\text{Sr}_{0.8}\text{TiO}_3$ and $\text{Ce}_{0.8}\text{Gd}_{0.2}\text{O}_2$ (GDC) on the impedance spectra and found that the content of GDC has a significant effect on polarization behavior. The values reported in this study are comparable with the optimal polarization resistance of $2.8 \Omega \text{ cm}^2$ measured in H_2 at 800 °C. The duration of the cell in the presence of 10,000 ppm H_2S is shown in Fig. 10d. The performance is relatively stable at 0.7 V. A current density of 184 mA cm^{-2} was observed and no sharp performance decrease was seen. Surprisingly, there was no change for at least one hour and there is gradual degradation to 157 mA cm^{-2} within 10 h. Sulfur can be absorbed by the oxygen-deficient surface sites, because of the lower oxidation state of non-stoichiometric oxygen [52]. Therefore, it has better sulfur tolerance than the nickel-based electrode. The LST–YSZ composite anode demonstrated potential use at a high concentration of H_2S .

4 Conclusions

$\text{La}_{0.4}\text{Sr}_{0.6}\text{TiO}_3$ was prepared using the solid-state reaction method and calcined in air at 1400 °C to investigate the performance of the anode of SOFCs. LST–YSZ composite anodes were also sintered in air at different temperatures. The three-electrode overpotential tests were practical, so as to characterize the properties of the anode. It was shown

that the performance of the LST–YSZ composite anode depended strongly on the YSZ content and the sintering temperature. The composite anode with a 60 wt% YSZ that was sintered at 1350 °C exhibited the lowest anode overpotential and the lowest polarization resistance of $0.26 \Omega \text{ cm}^2$ in 97% $\text{H}_2/3\%\text{H}_2\text{O}$. The LST–YSZ composite anode demonstrated excellent electrochemical performance in a high concentration of H_2S (10,000 ppm) containing H_2 , which is comparable with H_2 without sulfur. The LST powder prepared in air has the potential for application with SOFCs.

Supplementary Information The online version contains supplementary material available at <https://doi.org/10.1007/s10800-021-01568-8>.

Acknowledgements This work was supported by Sichuan Science and Technology Program (Grant Nos. 2019YFH0177 and 2021YFH0092); the talent introduction plan of Sichuan University of Science and Engineering (Grant Nos. 2016RCL36 and 2016RCL37); and Zigong Science and Technology Program (Grant Nos. 2019YYJC24 and 2020YGJC18).

References

- Onda K, Iwanari T, Miyauchi N, Ito K, Ohba T, Sakaki Y, Nagata S (2003) Cycle analysis of combined power generation by planar SOFC and gas turbine considering cell temperature and current density distributions. *J Electrochem Soc* 150:A1569
- Kendall K (2000) Hopes for a flame-free future. *Nature* 404:233–235
- McIntosh S, Gorte RJ (2004) Direct hydrocarbon solid oxide fuel cells. *Chem Rev* 104:4845–4866
- Aruna ST, Muthuraman M, Patil KC (1998) Synthesis and properties of Ni-YSZ cermet: anode material for solid oxide fuel cells. *Solid State Ion* 111:45–51
- Jacobson AJ (2010) Materials for solid oxide fuel cells. *Chem Mater* 22:660–674
- Han F, Mücke R, Van Gestel T, Leonide A, Menzler NH, Buchkremer HP, Stöver D (2012) Novel high-performance solid oxide fuel cells with bulk ionic conductance dominated thin-film electrolytes. *J Power Sources* 218:157–162
- Jiang SP, Chan SH (2004) A review of anode materials development in solid oxide fuel cells. *J Mater Sci* 39:4405–4439
- Mori M (1998) Thermal expansion of nickel-zirconia anodes in solid oxide fuel cells during fabrication and operation. *J Electrochem Soc* 145:1374–1381
- Presto S, Barbucci A, Carpanese MP, Viviani M, Marazza R (2009) Electrochemical performance of Ni-based anodes for solid oxide fuel cells. *J Appl Electrochem* 39:2257–2264
- Matsuzaki Y, Yasuda I (2000) The poisoning effect of sulfur-containing impurity gas on a SOFC anode: Part I. Dependence on temperature, time, and impurity concentration. *Solid State Ionics* 132:261–269
- Sapountzi FM, Brosda S, Papazisi KM, Balomenou SP, Tsipplakides D (2012) Electrochemical performance of $\text{La}_{0.75}\text{Sr}_{0.25}\text{Cr}_{0.9}\text{Mn}_{0.1}\text{O}_3$ perovskites as SOFC anodes in CO/CO_2 mixtures. *J Appl Electrochem* 42:727–735
- Karczewski J, Riegel B, Molin S, Winiarski A, Gazda M, Jasinski P, Murawski L, Kusz B (2009) Electrical properties of $\text{Y}_{0.08}\text{Sr}_{0.92}\text{Ti}_{0.92}\text{Nb}_{0.08}\text{O}_{3-\delta}$ after reduction in different reducing conditions. *J Alloys Compd* 473:496–499

13. Kumar P, Presto S, Sinha ASK, Varma S, Viviani M, Singh P (2017) Effect of samarium (Sm^{3+}) doping on structure and electrical conductivity of double perovskite $\text{Sr}_2\text{NiMoO}_6$ as anode material for SOFC. *J Alloys Compd* 725:1123–1129
14. Zhou X, Yan N, Chuang KT, Luo J (2014) Progress in La-doped SrTiO_3 (LST)-based anode materials for solid oxide fuel cells. *RSC Adv* 4:118–131
15. Torabi A, Etsell TH (2013) Electrochemical behavior of solid oxide fuel cell anodes based on infiltration of Y-doped SrTiO_3 . *J Power Sources* 225:51–59
16. Hui S, Petric A (2002) Electrical properties of yttrium-doped strontium titanate under reducing conditions. *J Electrochem Soc* 149:J1–J10
17. Ma Q, Tietz F (2012) Comparison of Y and La-substituted SrTiO_3 as the anode materials for SOFCs. *Solid State Ion* 225:108–112
18. Marina OA, Canfield NL, Stevenson JW (2002) Thermal, electrical, and electrocatalytic properties of lanthanum-doped strontium titanate. *Solid State Ion* 149:21–28
19. Moos R, Härdtl KH (1996) Electronic transport properties of $\text{Sr}_{1-x}\text{La}_x\text{TiO}_3$ ceramics. *J Appl Phys* 80:393–400
20. Moos R, Bischoff T, Menesklou W, Härdtl KH (1997) Solubility of lanthanum in strontium titanate in oxygen-rich atmospheres. *J Mater Sci* 32:4247–4252
21. Xu J, Zhou X, Dong X, Pan L, Sun K (2017) Catalytic activity of infiltrated $\text{La}_{0.3}\text{Sr}_{0.7}\text{Ti}_{0.3}\text{Fe}_{0.7}\text{O}_{3-\delta}\text{-CeO}_2$ as a composite SOFC anode material for H_2 and CO oxidation. *Int J Hydrogen Energy* 42:15632–15640
22. Xu J, Zhou X, Cheng J, Pan L, Wu M, Dong X, Sun K (2017) Electrochemical performance of highly active ceramic symmetrical electrode $\text{La}_{0.3}\text{Sr}_{0.7}\text{Ti}_{0.3}\text{Fe}_{0.7}\text{O}_{3-\delta}\text{-CeO}_2$ for reversible solid oxide cells. *Electrochim Acta* 257:64–72
23. Shahid M, He C, Sankarasubramanian S, Ramani V, Basu S (2020) Enhanced methane electrooxidation by ceria and nickel oxide impregnated perovskite anodes in solid oxide fuel cells. *Int J Hydrogen Energy* 45:11287–11296
24. Presto S, Barbucci A, Carpanese MP, Han F, Costa R, Viviani M (2018) Application of La-doped SrTiO_3 in advanced metal-supported solid oxide fuel cells. *Crystals* 8:134
25. Huang X, Zhao H, Qiu W, Wu W, Li X (2007) Performances of planar solid oxide fuel cells with doped strontium titanate as anode materials. *Energy Convers Manag* 48:1678–1682
26. Lee S, Kim G, Vohs JM, Gorte RJ (2008) SOFC Anodes Based on Infiltration of $\text{La}_{0.3}\text{Sr}_{0.7}\text{TiO}_3$. *J Electrochem Soc* 155:B1179
27. Yurkiv V, Constantin G, Hornes A, Gondolini A, Mercadelli E, Sanson A, Dessemond L, Costa R (2015) Towards understanding surface chemistry and electrochemistry of $\text{La}_{0.1}\text{Sr}_{0.9}\text{TiO}_{3-\alpha}$ based solid oxide fuel cell anodes. *J Power Sources* 287:58–67
28. Gondolini A, Mercadelli E, Constantin G, Dessemond L, Yurkiv V, Costa R, Sanson A (2018) On the manufacturing of low temperature activated $\text{Sr}_{0.9}\text{La}_{0.1}\text{TiO}_{3-\delta}\text{-Ce}_{1-x}\text{Gd}_x\text{O}_{2-\delta}$ anodes for solid oxide fuel cell. *J Eur Ceram Soc* 38:153–161
29. Koo J-H, Lee K-T (2016) The effect of firing conditions on electrical conductivity and electrochemical properties of $\text{Sr}_{0.8}\text{La}_{0.2}\text{TiO}_3\text{-Ce}_{0.9}\text{Gd}_{0.1}\text{O}_{1.95}$ composite anodes for solid oxide fuel cells. *Ceram Int* 42:2209–2213
30. Roushanafshar M, Luo J-L, Vincent AL, Chuang KT, Sanger AR (2012) Effect of hydrogen sulfide inclusion in syngas feed on the electrocatalytic activity of LST-YDC composite anodes for high temperature SOFC applications. *Int J Hydrogen Energy* 37:7762–7770
31. Hashimoto S, Kindermann L, Poulsen FW, Mogensen M (2005) A study on the structural and electrical properties of lanthanum-doped strontium titanate prepared in air. *J Alloys Compd* 397:245–249
32. Cimenti M, Co AC, Birss VI, Hill JM (2007) Distortions in electrochemical impedance spectroscopy measurements using 3-electrode methods in SOFC. I—effect of cell geometry. *Fuel Cells* 7:364–376
33. Esquirol A, Brandon NP, Kilner JA, Mogensen M (2004) Electrochemical characterization of $\text{La}_{0.6}\text{Sr}_{0.4}\text{Co}_{0.2}\text{Fe}_{0.8}\text{O}_3$ cathodes for intermediate-temperature SOFCs. *J Electrochem Soc* 151:A1847
34. Jørgensen MJ, Mogensen M (2001) Impedance of solid oxide fuel cell LSM/YSZ composite cathodes. *J Electrochem Soc* 148:A433
35. Shahid M, Ramani V, Basu S (2020) Kinetics of methane electrooxidation in pure and composite anodes of $\text{La}_{0.3}\text{Y}_{0.1}\text{Sr}_{0.4}\text{TiO}_{3-\delta}$. *J Solid State Electrochem* 24:145–156
36. Yoo KB, Choi GM (2011) LST–GDC composite anode on LaGaO_3 -based solid oxide fuel cell. *Solid State Ion* 192:515–518
37. Jiang SP (2004) Cell configuration for performance evaluation in planar solid oxide fuel cells. *J Appl Electrochem* 34:1045–1055
38. Zhang L, Jiang SP, Wang W, Zhang YJ (2007) NiO/YSZ, anode-supported, thin-electrolyte, solid oxide fuel cells fabricated by gel casting. *J Power Sources* 170:55–60
39. Matsushima T, Ohru H, Hirai T (1998) Effects of sinterability of YSZ powder and NiO content on characteristics of Ni-YSZ cermets. *Solid State Ion* 111:315–321
40. Kofenstein R, Jager L, Zenkner M, Muller T, Abicht HP (2008) Shrinkage mechanism and phase evolution of fine-grain BaTiO_3 powder compacts containing 10 mol% BaGeO_3 prepared via a precursor route. *Mater Chem Phys* 112:531–535
41. Li X, Zhao H, Zhou X, Xu N, Xie Z, Chen N (2010) Electrical conductivity and structural stability of La-doped SrTiO_3 with A-site deficiency as anode materials for solid oxide fuel cells. *Int J Hydrogen Energy* 35:7913–7918
42. Sun X, Wang S, Wang Z, Ye X, Wen T, Huang F (2008) Anode performance of LST-x CeO_2 for solid oxide fuel cells. *J Power Sources* 183:114–117
43. Kusy RP (1977) Influence of particle size ratio on the continuity of aggregates. *J Appl Phys* 48:5301–5305
44. Kim J-D, Kim G-D, Moon J-W, Lee H-W, Lee K-T, Kim C-E (2000) The effect of percolation on electrochemical performance. *Solid State Ion* 133:67–77
45. Mukundan R, Brosha EL, Garzon FH (2004) Sulfur tolerant anodes for SOFCs. *Electrochem Solid-State Lett* 7:A5–A7
46. Cheng Z, Wang J-H, Choi Y, Yang L, Lin MC, Liu M (2011) From Ni-YSZ to sulfur-tolerant anode materials for SOFCs: electrochemical behavior, in situ characterization, modeling, and future perspectives. *Energy Environ Sci* 4:4380–4409
47. Zha S, Cheng Z, Liu M (2007) Sulfur poisoning and regeneration of Ni-based anodes in solid oxide fuel cells. *J Electrochem Soc* 154:B201–B206
48. Afshar MR, Yan N, Zahiri B, Mitlin D, Chuang KT, Luo J-L (2015) Impregnation of $\text{La}_{0.4}\text{Ce}_{0.6}\text{O}_{1.8}\text{-La}_{0.4}\text{Sr}_{0.6}\text{TiO}_3$ as solid oxide fuel cell anode in H_2S -containing fuels. *J Power Sources* 274:211–218
49. Cheng Z, Zha SW, Liu ML (2007) Influence of cell voltage and current on sulfur poisoning behavior of solid oxide fuel cells. *J Power Sources* 172:688–693
50. Vincent AL, Luo JL, Chuang KT, Sanger AR (2011) Promotion of activation of CH_4 by H_2S in oxidation of sour gas over sulfur tolerant SOFC anode catalysts. *Appl Catal B* 106:114–122
51. Rath MK, Lee K-T (2016) Properties and electrochemical performance of $\text{Sr}_{0.8}\text{La}_{0.2}\text{TiO}_{3-\delta}\text{-Ce}_{0.8}\text{Gd}_{0.2}\text{O}_{2-\delta}$ composite anodes for intermediate temperature solid oxide fuel cells. *J Alloys Compd* 657:537–545
52. Arrivé C, Delahaye T, Joubert O, Gauthier GH (2019) Study of (La,Sr)(Ti,Ni) $\text{O}_{3-\delta}$ materials for symmetrical solid oxide cell electrode—Part A: synthesis and structure analysis in air. *Ceram Int* 45:17969–17977

Authors and Affiliations

Jiaqi Cheng¹ · Junyi Gong¹ · Shuai Yue¹ · Yao Jiang¹ · Xiangjun Hou¹ · Jianjun Ma¹ · Yali Yao² · Cairong Jiang¹ 

¹ School of Materials Science and Engineering, Sichuan University of Science and Engineering, Zigong 643000, Sichuan, People's Republic of China

Christiaan de Wet & Pioneer Road, Private Bag X6, Florida 1710, South Africa

² Institute for the Development of Energy for African Sustainability (IDEAS), University of South Africa, cnr